

1     **Direct, Efficient and Selective Capture of Low Concentration of CO<sub>2</sub> from Natural Gas**  
2             **Flue Gas Using a High Temperature Tubular Carbon Capture Membrane**

3                     Shichen Sun, Aidan Billings, Kangkang Zhang, Kevin Huang\*

4     Department of Mechanical engineering, University of South Carolina, Columbia, SC, 29212

5                     \*Corresponding author: [huang46@cec.sc.edu](mailto:huang46@cec.sc.edu)

6

7                                     **Abstract**

8     Natural gas (NG) fired power plants emit low concentration (4-5%) of CO<sub>2</sub>, which presents  
9     additional technical and economic challenges to the current benchmark amine absorption  
10    technology. The newly emerged high-temperature multiphase membranes operated on molten  
11    carbonate (MC) chemistry for CO<sub>2</sub> capture/separation/conversion have been demonstrated with  
12    great potential to meet this challenge. In this study, we report on the CO<sub>2</sub> capture performance of  
13    such a membrane in tubular geometry from a mockup NG flue gas. The membrane is comprised  
14    of a mixture of Gd<sub>0.20</sub>Ce<sub>0.80</sub>O<sub>1.95</sub> (GDC) and MC, in which GDC forms a porous skeleton to contain  
15    MC. We show that the membrane with a dimension of 6.1 mm in outer diameter, 5.1 mm in inner  
16    diameter and 5 cm in effective length (resulting in 4 cm<sup>2</sup> effective surface area) can achieve a CO<sub>2</sub>  
17    flux density of 0.46-0.55 mL/min·cm<sup>2</sup> at 650 °C, capturing 97% pure CO<sub>2</sub> at a rate of 37-42% from  
18    5%CO<sub>2</sub>-N<sub>2</sub> using moistened Ar as the sweep gas. The level of performance demonstrated by this  
19    study suites the membrane well for stationary CO<sub>2</sub> capture from NG power plants.

20    **Keywords:** Membrane; CO<sub>2</sub> flux; CO<sub>2</sub> purity; CO<sub>2</sub> capturing rate; H<sub>2</sub>O enhancement.

21

## 1. Introduction

Natural gas (NG) fired power plants have surpassed coal fired power plants and become the #1 source of electricity generation in the U.S. in 2019, producing 1.6 billion MWhs or 40.3% of the national electricity supply (vs. 19.3% for coal-fired power plants) [1]. The widespread use of NG is primarily driven by the availability of low-cost shale gas, high efficiency of natural gas combined cycle (NGCC) technology, and growing concerns on CO<sub>2</sub>/CH<sub>4</sub> related global warming. With NG as a cleaner fuel, the CO<sub>2</sub> emissions are ~40% less than burning coals. Additionally, there is no emissions of Hg and chloride, and PM, NO<sub>x</sub>, and SO<sub>x</sub> emissions are all at or below the federal regulatory limits currently in effect for NGCC technology.

Although NGCC power plants emit less CO<sub>2</sub>, the total amount of CO<sub>2</sub> annually released to the atmosphere is still staggering. In 2019 alone, the U.S. released ~0.9 billion tons of CO<sub>2</sub> from NGCC power plants to the atmosphere [2]. To control global carbon pollution, this source of CO<sub>2</sub> emissions must be curtailed. The current benchmarks of CO<sub>2</sub>-capture/separation technologies are principally based on reversible chemical/physical sorption processes, using liquid solvents and solid sorbents as CO<sub>2</sub> scrubbers [3-5]. However, the cost and energy penalty to implement these scrubbing technologies into existing power plants are still too high for practical applications. For example, implementing Shell CONSOLV, a benchmark regeneratable “amine absorption” technology, into a 740 MWe NGCC power plant would lower the plant’s net efficiency from 53.6% to 47.7% at 90% CO<sub>2</sub> capture capacity and incur a 64% (from \$43.3/MWh to \$70.9/MWh, excluding T&S) hike in LCOE over the baseline case [6]. Therefore, to achieve flue gas carbon capture at a large commercial scale, new transformational carbon capture technologies with lower cost and energy consumption are highly desirable.

1 Unlike solvent- and sorbent-based CO<sub>2</sub> capture techniques, membrane-based CO<sub>2</sub> capture  
2 processes present fundamental advantages in cost and energy consumption due to their capability  
3 of delivering high-pressure CO<sub>2</sub>, promoting CO shifting reactions, and not using energy-intensive  
4 steam or chemical loads [7-17]. However, the major issues with these size-exclusion and  
5 solubility-diffusivity based membranes are the tradeoff between selectivity and permeability, aka.  
6 the Robeson upper bound rule. Therefore, developing alternative new membrane technologies to  
7 capture CO<sub>2</sub> more selectively and efficiently is greatly needed.

8 An emerging class of carbon capture membranes, in recent years, are the multiphase solid/molten  
9 carbonate (MC) composites [18-24]. This family of carbon transport membranes (CTMs) operates  
10 on high-temperature chemistries of ions, or mixed ion/electron transports, without the limitation  
11 of Robeson rule [25, 26]. Initial laboratory results have shown the great potential of CTMs with  
12 high CO<sub>2</sub> flux and selectivity in 600-900 °C [18, 20, 21, 27, 28]. The operating temperature of  
13 these CTMs also matches well with that of the flue-gas at the exit of gas turbine cycle in a NGCC,  
14 thus allowing the heat in the flue-gas to be directly utilized for membrane operation. By design,  
15 the membrane reactor can be practically inserted between the gas turbines and the heat recovery  
16 steam generators (HRSG) to directly capture hot CO<sub>2</sub>, without changing the flue gas temperature  
17 (~650°C) for the downstream HRSG and steam turbine cycle, thus potentially saving energy and  
18 cost.

19 In this study, we show that a promising tubular ceramic (Gd<sub>0.20</sub>Ce<sub>0.80</sub>O<sub>1.95</sub> (GDC))-molten  
20 carbonate (MC) dual-phase membrane can efficiently and selectively capture 5% CO<sub>2</sub> from a  
21 mockup natural gas flue gas at 650 °C. Compared to conventional disk-type CTM membranes,  
22 tubular membranes have advantages in CO<sub>2</sub> capture efficiency (less bypass), easy gas sealing, and  
23 tolerance to stresses. [29-33] We particularly emphasize the beneficial effect of steam on the CO<sub>2</sub>

1 flux density and capture efficiency, given the fact that there is easy access to steam in NGCC  
2 power plants.

## 3 **2. Experimental procedure**

### 4 *Preparation of GDC-MC Dual Phase Tubular Membrane*

5 The GDC porous tubular membrane was fabricated via a cold-isostatic press (CIP) method. Briefly,  
6  $\text{Gd}_{0.20}\text{Ce}_{0.80}\text{O}_{1.95}$  (GDC-20M, Fuelcellmaterials) powder was first intimately mixed with carbon  
7 black as a pore former, with a volume ratio of 1:1, in ethanol by ball-milling for 24 h. After mixing  
8 and drying, the powder mixture was densely packed into a rubber mold, with a stainless-steel rod  
9 as insert, and a flat cap sealed on top. The powder mixture was then pressed under 150 MPa for  
10 30 minutes in a CIP. After pressing, the tube was removed from the mold and slightly polished on  
11 its surface with sandpaper. It was then sintered at 600°C for 2 h in air, to remove the carbon pore  
12 former, and then 1200 °C for 5 h to achieve good mechanical strength.

13 MC infiltration for the GDC tubular membrane was carried out ex-situ. First, the open end of the  
14 GDC tubular membrane was tied to a platinum string, and a porous alumina cylinder was inserted  
15 to adsorb any MC that flowed into the membrane, preventing the formation of a detrimental MC  
16 overlayer. The tubular membrane assembly was then heated to 550 °C at 1°C/min in a furnace,  
17 hanging above a crucible filled with a eutectic mixture of  $\text{Li}_2\text{CO}_3$  ( $\geq 99\%$ , Alfa Aesar) and  $\text{Na}_2\text{CO}_3$   
18 ( $\geq 99\%$ , Alfa Aesar) in a molar ratio of 52:48. Upon reaching 550 °C, the membrane was slowly  
19 dropped into the MC, with the closed-end facing down, and then kept for 30 minutes. After that,  
20 the membrane was slowly pulled up from the MC, and the porous alumina tube was removed from  
21 the membrane, followed by cooling to room temperature at 1 °C/min. After infiltration, both sides

1 of the tubular membrane were gently polished with sandpaper to remove the residual carbonate  
2 overlayer.

### 3 *Characterization of Membranes*

4 The phase structures of GDC tubular membrane after sintering and infiltration were examined with  
5 X-ray diffraction (XRD, Rigaku D/MAX-2100) with Cu K $\alpha$  radiation ( $\lambda = 1.5418 \text{ \AA}$ ) from 20°-  
6 80°. Relative densities ( $\epsilon$ ) of the sintered porous GDC tubes were determined by the Archimedes'  
7 method. To obtain other microstructure measurements of the porous matrix, e.g. tortuosity ( $\tau$ ) and  
8 average pore radius ( $r$ ), we used a helium permeation method as described in previous works. [34,  
9 35] Briefly, a porous GDC tube was first sealed to a stainless-steel sample holder with a silicone  
10 paste, which was then inserted into a chamber connected to a helium cylinder and a mass flow  
11 controller. The downstream pressure ( $P_L$ ) of the membrane was varied via an outlet valve, while  
12 the pressure difference across the membrane ( $\Delta P$ ), the inlet pressure of the membrane ( $P_I$ ), and the  
13 flow rate ( $f$ ) are simultaneously recorded with a pressure differential gauge, pressure gauge, and  
14 bubble flow meter, respectively.

15 The permeance of helium,  $F$ , through the porous matrix is calculated by

$$16 \quad F = \left( \frac{Q}{S \cdot (P_I - P_L)} \right) \quad (1)$$

17 where  $S$  is the active area for the permeating gas and  $Q$  is the molar flow rate of permeating helium  
18 calculated from the bubble flow meter.

19 According to Darcy's law,  $F$  is given by

$$20 \quad F = \alpha + \beta \cdot \left( P_I - \frac{\Delta P}{2} \right) \quad (2)$$

1 where  $\alpha$  and  $\beta$  are permeability coefficients related to Knudsen flow and viscous flow, respectively.

2 The pore radius,  $r$ , is then calculated by

$$3 \quad r = 8.4818\mu \sqrt{\frac{RT}{M_w} \left(\frac{\beta}{\alpha}\right)} \quad (3)$$

4 where  $R$  is the gas constant,  $T$  is absolute temperature, and  $M_w$  is the molecular weight of helium.

5 Since  $\alpha$  and  $\beta$  are related to  $\varepsilon/\tau$  by the following equations

$$6 \quad \alpha = 1.06 \left(\frac{\varepsilon}{\tau}\right) \left(\frac{r}{L\sqrt{RTM_w}}\right) \quad (4)$$

$$7 \quad b = 0.125 \left(\frac{\varepsilon}{\tau}\right) \left(\frac{r^2}{L\mu RT}\right) \quad (5)$$

8 where  $L$  is the thickness of the porous matrix and  $\mu$  is the viscosity of helium,  $\tau$  can be further  
9 calculated from the known porosity ( $\varepsilon$ ) and  $r$  values.

10 The microstructure of the GDC-MC tubular membranes after sintering, infiltration, and tests were  
11 carefully examined by a field emission scanning electron microscope (FESEM, Zeiss GeminiSEM  
12 500) and energy dispersive spectroscopy (EDS, AMETEK, EDAX ELECT SUPER) at an  
13 accelerating voltage of 5 kV and an acquisition time of 300 seconds, and the phase purity of GDC-  
14 MC tubular membranes after tests were analyzed by same X-ray diffraction (XRD, Rigaku  
15 D/MAX-2100) under the same condition as described above.

### 16 *Tubular Membrane Assembly*

17 We used a homemade fixture for membrane performance testing in capturing/separating  $\text{CO}_2$ ; the  
18 setup is schematically shown in Figure 1. To assemble the test article, the one-end closed tubular  
19 membrane was first mounted and sealed onto an alumina supporting tube with silver paste,  
20 followed by curing at 150 °C for 2 hours. The sealed tubular membrane was then placed

1 horizontally inside a quartz tube with flanges on both ends in a tubular furnace. The outer surface  
2 of the tubular membrane, or the permeate surface, was fed with the sweep gas Ar, and the inner  
3 surface, or the retentate surface, was fed with CO<sub>2</sub>-N<sub>2</sub> mixture. To avoid gas bypass, the free  
4 volume inside the quartz tube was occupied by thermal blocks (insulation materials) wrapped with  
5 ceramic wool, forcing Ar to flow over the outer surface of the membrane. The sweep Ar was also  
6 moistened by a humidifier and the water content in Ar was measured online by a humidity sensor  
7 (Vaisala model 332). The composition of sweep effluent was analyzed by a micro-GC (Agilent  
8 MicroGC-490). The same humidity sensor was also switchable to the feed gas line for detecting  
9 water content transported through the transmembrane.

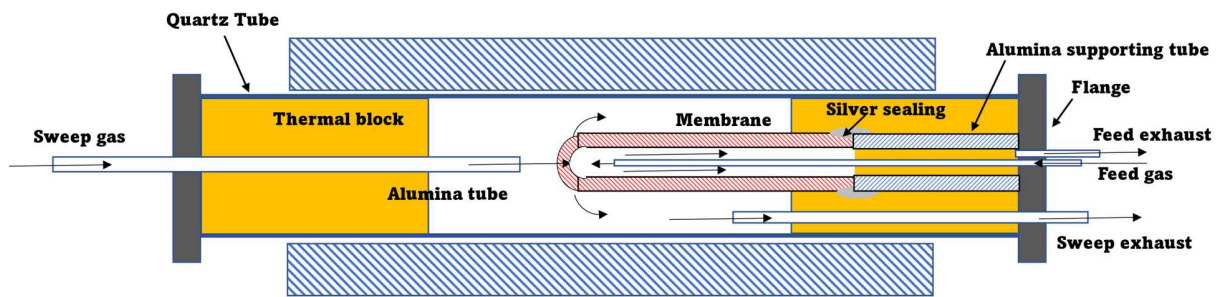


Figure 1. Schematic of GDC-MC tubular membrane testing setup

### CO<sub>2</sub> Flux Measurements

14 To examine the effect of the partial pressure of steam ( $p_{H_2O}$ ) on the CO<sub>2</sub> flux, a range of steam  
15 contents (0-15%) were generated by passing the Ar permeate gas through a homemade water  
16 saturator at different temperatures before the gas was fed to the outside of the tube. Simultaneously,  
17 a simulated flue gas mixture of 95%N<sub>2</sub>/5%CO<sub>2</sub> at a flow rate of 100 mL/min was fed to the inner  
18 surface of the membrane as the retentate gas. The real steam contents in the carrier gas and in the  
19 retentate exhaust were determined by the on-line humidity sensor.

1 To examine the effect of the partial pressure of CO<sub>2</sub> ( $p_{CO_2}$ ) in the retentate gas on the CO<sub>2</sub> flux,  
2 the CO<sub>2</sub> concentration in N<sub>2</sub> was varied between 5, 15, and 50%, with a fixed total flow rate of 100  
3 mL/min. The permeate gas for this study was Ar at a flow rate of 100 mL/min saturated with  
4 3% H<sub>2</sub>O.

5 Finally, to examine the short-term stability of the membrane under different flow rate conditions,  
6 we used 80, 100, and 150 mL/min Ar flows saturated with 3% H<sub>2</sub>O, while keeping the total flow  
7 rate on the retentate side the same to avoid possible influence from pressure difference, i.e.,  
8 80/100/150 mL/min, with a fixed composition of 95% N<sub>2</sub>/5% CO<sub>2</sub>.

9 In all flux measurement tests, the temperature was fixed at 650 °C. The composition of the  
10 permeate side effluent was analyzed by an online gas chromatographer (Micro-GC 490, Agilent).  
11 At each condition ( $p_{H_2O}/p_{CO_2}$ /flow rate), one hour was given to ensure full stability before data  
12 was taken. The final CO<sub>2</sub> and N<sub>2</sub> flux densities (as an indicator of leakage) permeated through the  
13 membrane were calculated using the following equations:

$$14 \quad J_{CO_2} = \frac{C_{CO_2} - C_{Leak}}{1 - C_{CO_2} - C_{N_2}} \times \frac{F_{Ar}}{A} \quad (6)$$

$$15 \quad J_{N_2} = \frac{C_{N_2}}{1 - C_{CO_2} - C_{N_2}} \times \frac{F_{Ar}}{A} \quad (7)$$

16 where  $F_{Ar}$  is the flow rate of the Ar permeate gas, A is the effective area of the membrane,  $C_{CO_2}$  and  
17  $C_{N_2}$  is the measured concentration of CO<sub>2</sub> and N<sub>2</sub> in permeate exhaust, respectively. To correct for  
18 the leakage through the membrane, the CO<sub>2</sub> flux was corrected by subtracting  $C_{Leak}$ , which equals  
19  $C_{N_2} * \left( \frac{p_{CO_2}}{1 - p_{CO_2}} \right)$ .

20 The CO<sub>2</sub> capture rate (CCR) was also calculated via the following equation:

1 
$$CCR = \frac{C_{CO_2} - C_{Leak}}{p_{CO_2} * F_{feed}} \times \frac{F_{Ar}}{A} \times \frac{1}{1 - C_{CO_2} - C_{N_2}} \quad (8)$$

2 where  $p_{CO_2}$  and  $F_{feed}$  are the partial pressure of CO<sub>2</sub> and the flow rate of the retentate gas mixture,  
3 respectively.

4 In addition, the water flux through the membrane, from the permeate side to retentate side, was  
5 also calculated:

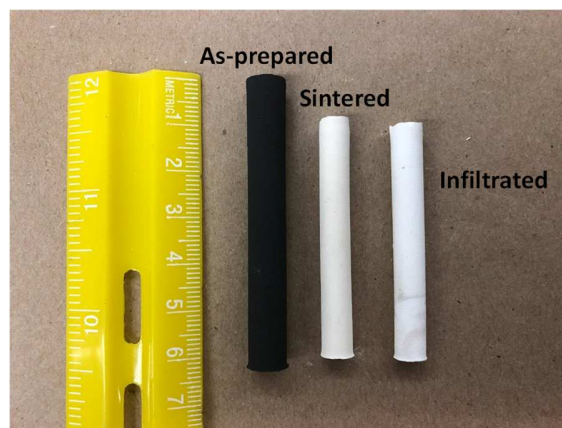
6 
$$J_{H_2O} = \frac{C_{H_2O} * F_{feed}}{A} \quad (9)$$

7 where  $C_{H_2O}$  is the concentration of H<sub>2</sub>O in the retentate side effluent, analyzed by a humidity  
8 sensor.

9 **3. Results and discussions**

10 *Tubular membrane*

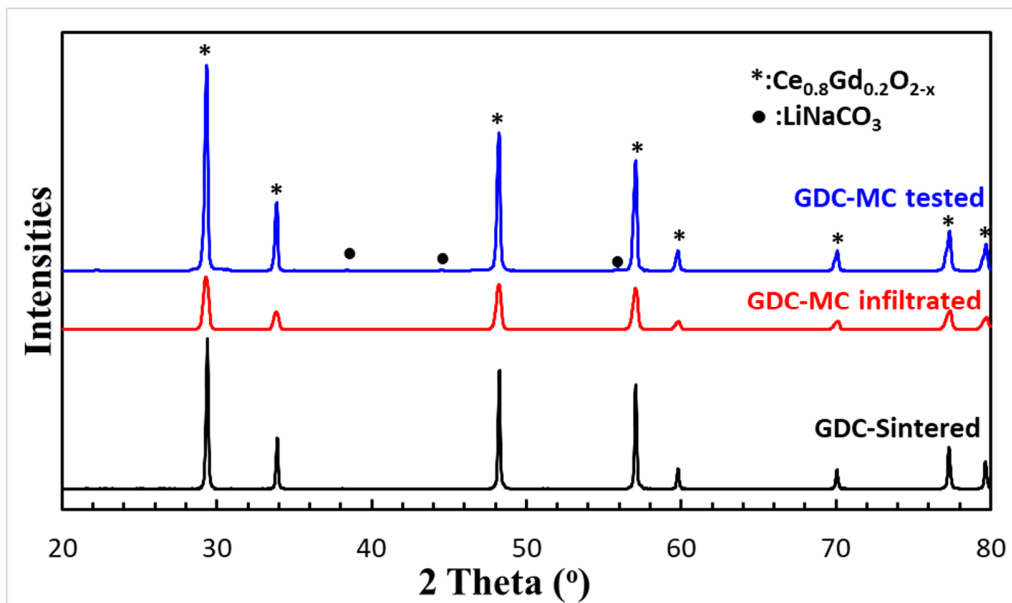
11 The physical image of the fabricated tubular membrane with one end closed is shown in Figure 2  
12 at different states. The final dimension of the sintered tubular membrane is 48 mm in length, 6.1  
13 mm in outer diameter, and 5.1 mm in inner diameter. After assembling the tube membrane on a  
14 supporting Al<sub>2</sub>O<sub>3</sub> tube with silver sealant, the resulting effective surface area is 4.0 cm<sup>2</sup>.



15

1 Figure 2. Picture of tubular membranes in the state of as-pressed, as-sintered, and after-  
2 infiltration from left to right, respectively.

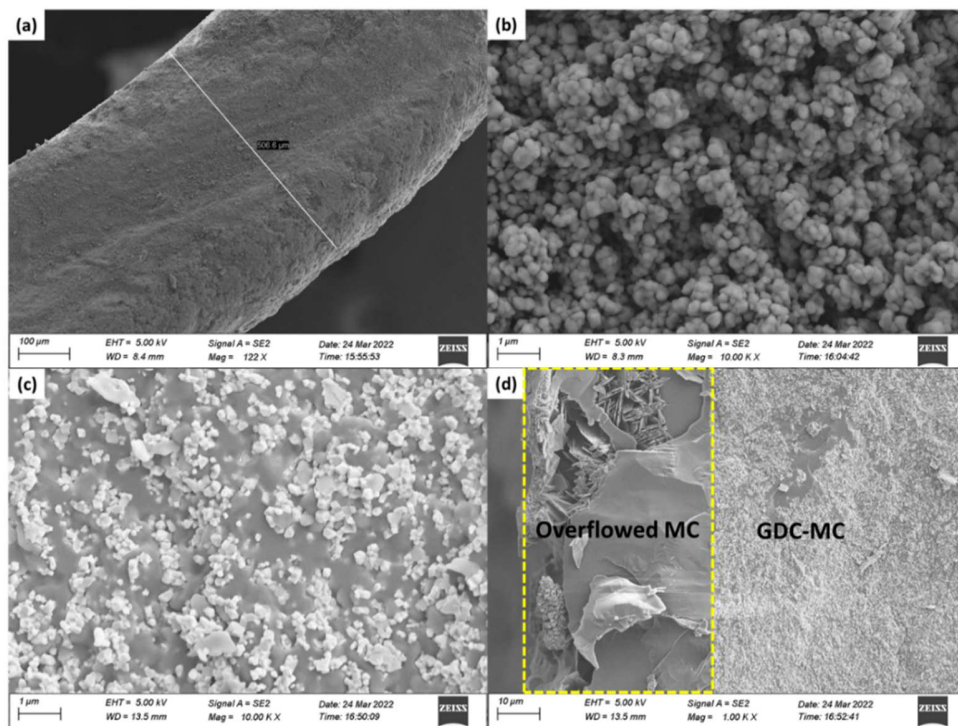
3 Figure 3 shows the XRD patterns of GDC tubular membrane after sintering at 1200 °C, after  
4 infiltration with MC and after testing. The GDC-20 ( $\text{Ce}_{0.8}\text{Gd}_{0.2}\text{O}_{2-x}$ ) peaks are well maintained  
5 after sintering and MC infiltration, while only trace amount of  $\text{LiNaCO}_3$  is detected in the crushed  
6 GDC-MC tubular membrane after testing. These observations suggest good chemical stability of  
7 GDC during the processing and testing process and good compatibility with MC. The porosity ( $\epsilon$ ),  
8 tortuosity ( $\tau$ ) and average pore diameter determined by Archimedes' method and helium  
9 permeation method are 30%, 1.94 and 0.27  $\mu\text{m}$ , respectively.



10  
11 Figure. 3 XRD patterns of GDC tubular membrane after sintering, infiltration, and testing.

12 Figure 4(a) shows the cross section of the membrane at lower magnification, indicating the  
13 thickness of the membrane is  $\sim 0.5$  mm. At higher magnification, Figure 4(b) shows that the  
14 membrane possesses a porous structure, with uniformly distributed pores at a pore size of  $< 1$   $\mu\text{m}$

1 after sintering at 1200 °C for 5 hours, which is consistent with the results obtained from helium  
2 permeation method. After infiltration of MC into the porous GDC skeleton, Figure 4(c) shows a  
3 dense microstructure with the pores in the GDC-MC skeleton filled with MC. It is worth  
4 mentioning that an obvious overlayer of carbonates can be seen in Figure 4(d) on some part of the  
5 inner surface of the membrane, which indicates that the inserted porous alumina cylinder did not  
6 fully absorb all overflowed MC. Therefore, it is necessary to carry out additional cleaning to  
7 remove the excess surface overlayer. We typically used warm water to wipe the membrane  
8 surfaces before flux testing. It is worth mentioning that such MC overlayer can also be minimized  
9 by controlling the infiltration time as demonstrated in the work [30].



10

11 Figure 4. Cross-section image of (a) and (b) GDC tubular membrane, (c) GDC-MC tubular  
12 membrane after MC infiltration, and (d) the inner side of GDC-MC membrane after infiltration  
13 (The excess MC is indicated within the dashed line).

1 *The effect of  $p_{H_2O}$  in permeate gas on  $J_{CO_2}$*

2 The effect of  $p_{H_2O}$  on the  $J_{CO_2}$  of the GDC-MC tubular membrane was studied at 650 °C and the  
3 results are shown in Figure 5. With 5%CO<sub>2</sub>-N<sub>2</sub> as the retentate gas and dry Ar as permeate gas,  
4  $J_{CO_2}$  stabilizes at ~0.35 mL/min·cm<sup>2</sup> with a CCR of ~28%. Such  $J_{CO_2}$  is in agreement with the  
5 calculated 0.378 mL/min·cm<sup>2</sup> by equation below: [36]

$$6 \quad J_{CO_2} = -\left(\frac{\varepsilon}{\tau}\right) \frac{RT}{4F^2L} \frac{\varphi\sigma_c(1-\varphi)\sigma_o}{\varphi\sigma_c+(1-\varphi)\sigma_o} \ln \frac{P'_{CO_2}}{P''_{CO_2}} \quad (10)$$

7 where  $\varepsilon$  and  $\tau$  are the porosity and the tortuosity of the porous GDC, respectively; R is the gas  
8 constant; T is the absolute temperature in K; F is Faraday's constant; L is the thickness of the  
9 membrane, ~0.05 cm;  $\varphi$  is the volume fraction of the MC phase;  $\sigma_c$  and  $\sigma_o$  are the conductivities  
10 of carbonate-ions and oxide-ions in S/cm, respectively;  $P'_{CO_2}$  and  $P''_{CO_2}$  are the partial pressures at  
11 the feed and permeate sides in Pa, respectively.

12 With  $p_{H_2O}=0.03$  atm in Ar permeate gas, both  $J_{CO_2}$  and CCR increase to ~0.45 mL/min·cm<sup>2</sup> and  
13 ~36%, respectively. With a further increase in  $p_{H_2O}$  to 0.06, 0.10 and 0.15 atm, both  $J_{CO_2}$  and  
14 CCR increase to ~0.46, ~0.48, ~0.55 mL/min·cm<sup>2</sup>, and ~37, ~38, ~42%, respectively. A low N<sub>2</sub>  
15 leakage at the level of ~0.01 mL/min·cm<sup>2</sup> was found in both dry and wet conditions, giving a high  
16 CO<sub>2</sub> purity of ~97% during the capture process. It is noted that  $J_{CO_2}$  remains rather stable until  
17  $p_{H_2O}$  increases to 15%, when some fluctuations are observed. We speculate that the change in  
18 flux upon switching to higher H<sub>2</sub>O content may represent the establishment of the equilibrium  
19 between H<sub>2</sub>O and MC.

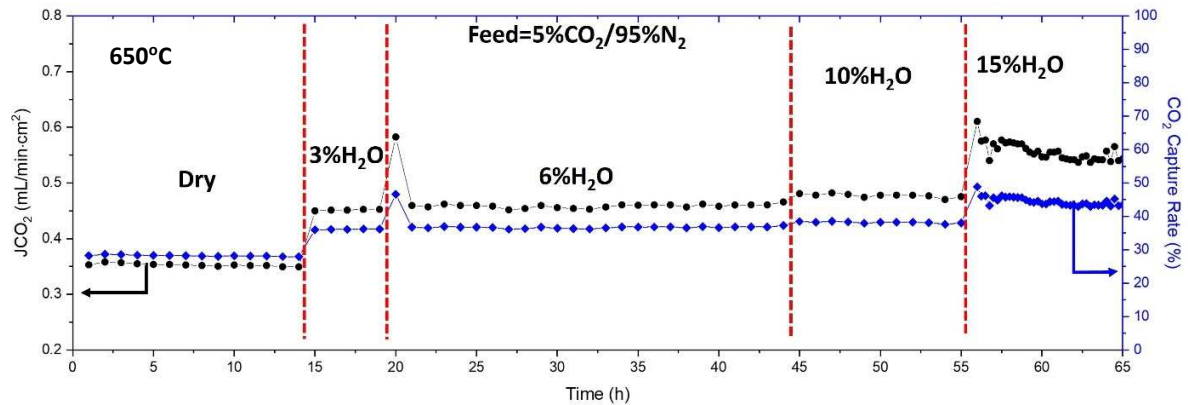
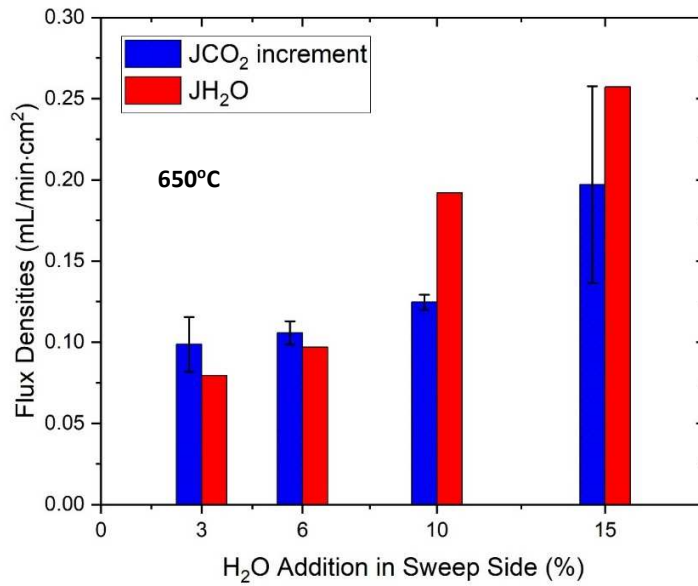


Figure 5.  $J_{CO_2}$  and CCR of a GDC-MC tubular membrane measured at 650 °C and various  $p_{H_2O}=0, 0.03, 0.06, 0.1$  and  $0.15$  atm with 5% $CO_2$ - $N_2$  as the retentate gas mixture.

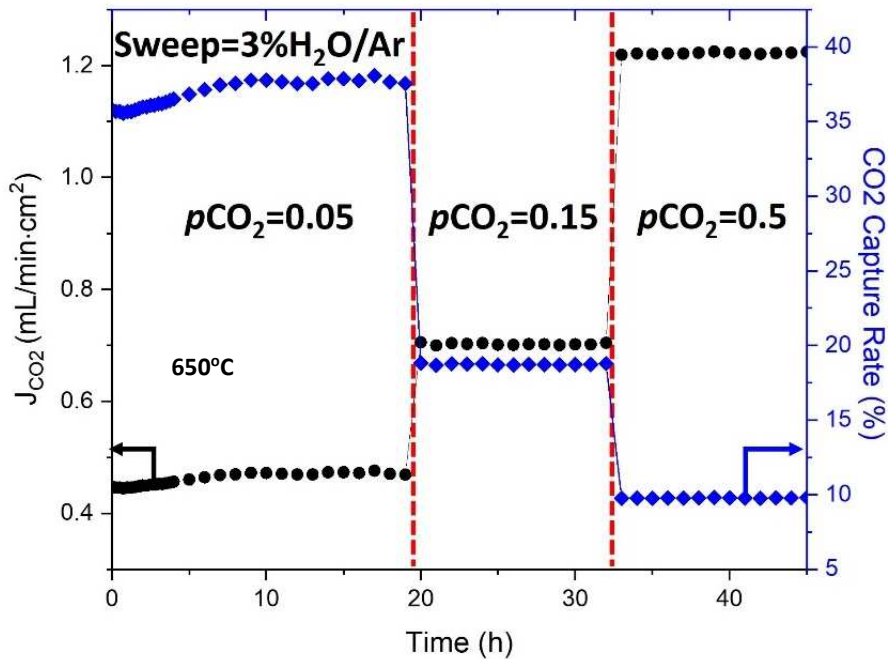
We have previously explained the  $H_2O$ -enhanced  $CO_2$  flux phenomenon by a  $CO_2/H_2O$  co-transport mechanism. [37] In this mechanism, the reaction between  $H_2O$  and  $CO_3^{2-}$  produces  $OH^-$ ; the latter moves in opposite direction of  $CO_3^{2-}$  in the MC phase, i.e. from the permeate side toward the retentate side, charge balancing  $CO_3^{2-}$ . At the retentate side surface,  $OH^-$  reaction with  $CO_2$ , forming  $H_2O$  and  $CO_3^{2-}$ . The counter-diffusion of  $OH^-$  accelerates  $CO_3^{2-}$ , thus enhancing  $CO_2$  flux. Based on this mechanism, the flux of  $CO_2$  at the permeate side should be equal to that of  $H_2O$  at the retentate side. To verify this hypothesis, we measured  $H_2O$  concentration in the effluent of the retentate gas and converted into flux. Figure 6 compares the measured  $J_{CO_2}$  and  $J_{H_2O}$ . At each  $H_2O$  content at the permeate side,  $J_{CO_2}$  and  $J_{H_2O}$  are comparable within a certain error bar. We speculate that the difference could be originated from  $H_2O$  content measurement. The humidity sensor typically has a higher uncertainty at higher  $H_2O$  contents. Nevertheless, the trend is clear, i.e. the higher the  $H_2O$  content in the permeate gas, the higher  $J_{H_2O}$  at the retentate gas effluent and  $J_{CO_2}$  in the permeate gas effluent, respectively.



1  
2 Figure 6.  $J_{CO_2}$  incremental and  $J_{H_2O}$  versus  $H_2O$  content measured at  $650^\circ C$  in permeate gas Ar.

3 *The effect of  $pCO_2$  in retentate gas on  $J_{CO_2}$*

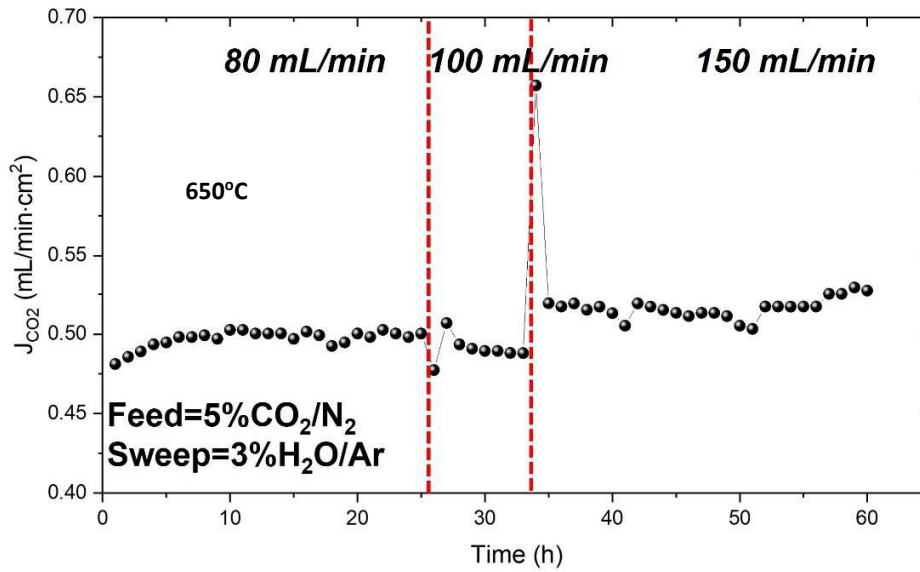
4 The effect of  $pCO_2$  in the retentate gas on the  $J_{CO_2}$  was also studied at  $650^\circ C$ . In this study, the Ar  
5 permeate gas was constantly saturated with 3%  $H_2O$ . The results are shown in Figure 7, where  $J_{CO_2}$   
6 and CCR are stabilized at  $\sim 0.43$  mL/min·cm<sup>2</sup> and 36% after  $\sim 20$  hours with a 5%  $CO_2$ - $N_2$  as the  
7 retentate gas. At  $pCO_2 = 0.15$  and  $0.50$ ,  $J_{CO_2}$  increases correspondingly to  $\sim 0.71$  and  $\sim 1.22$   
8 mL/min·cm<sup>2</sup>, while CCR decreases significantly to  $\sim 18\%$  and  $\sim 10\%$ , respectively. The decrease  
9 of CCR at higher  $pCO_2$  suggests that the small tubular membrane in use has limited capability of  
10 transporting all  $CO_2$  through the membrane of a definite surface area. To increase the CCR,  
11 increasing  $CO_2$  flux density or enlarging tube active area is needed; the latter is, however, a more  
12 expensive solution.



1  
 2 Figure 7. (a)  $J_{\text{CO}_2}$  and  $\text{CO}_2$  capture rate of a GDC-MC tubular membrane measured at 650 °C with  
 3 various  $p_{\text{CO}_2}=0.05, 0.15$  and  $0.5$  with  $3\%\text{H}_2\text{O}/\text{Ar}$  as the permeate gas.

4 *Short-term stability test*

5 The stability test on the membrane was carried out at 650 °C and different flow rates; the results  
 6 are shown in Figure 8. Despite two obvious changes at the switch of the flow rate, which is likely  
 7 related to the pressure change induced by flow rate change, no significant difference in  $J_{\text{CO}_2}$  was  
 8 found when the total flow rates of both retentate and permeate gases were varied simultaneously  
 9 from 80 to 100 mL/min, while there was a slight increase in  $J_{\text{CO}_2}$  (from  $\sim 0.48$  to  $\sim 0.51$  mL/min·cm<sup>2</sup>)  
 10 as the flow rate was increased to 150 mL/min. This finding suggests the limited capacity of the  
 11 membrane with a definite surface area to handle high mass flow of  $\text{CO}_2$ -containing stream. This  
 12 trend is in fact similar to the early finding in Figure 7 that CCR decreases with  $\text{CO}_2$  concentrations.



- 1
- 2 Figure 8.  $J_{\text{CO}_2}$  vs. time at different total flow rates on both retentate and permeate sides.
- 3 Temperature: 650 °C; retentate gas: 5%CO<sub>2</sub>-N<sub>2</sub>; permeate gas: 3%H<sub>2</sub>O-Ar.
- 4 Table 1 compares the results of this work with other tubular membranes of the same chemistry.
- 5 The GDC-MC tubular membrane of this study, with the largest effective area of 4 cm<sup>2</sup>
- 6 demonstrated, shows the best performance among all tubular CTM membranes, given the lowest
- 7 CO<sub>2</sub> concentration and intermediate temperature.
- 8 Table 1. Comparison of CO<sub>2</sub> permeation performance for different CTM tubular membranes.

Ceramic phase	Thickness (mm)	Area (cm <sup>2</sup> )	Feed $P_{\text{CO}_2}$ , atm	T (°C)	$J_{\text{CO}_2}$ (mL/min·cm <sup>2</sup> )	Ref.
La <sub>0.6</sub> Sr <sub>0.4</sub> Co <sub>0.8</sub> Fe <sub>0.2</sub> O <sub>3-δ</sub> (LSCF)	0.4	2.2	0.5	650-850	0.061-0.13	[38]
Yttria-stabilized zirconia (YSZ)	0.2–0.5	2.2	0.5	500-900	0.082-1.0	[39]
SrFe <sub>0.8</sub> Nb <sub>0.2</sub> O <sub>3-δ</sub> (SFN)	0.22	0.75	0.5	500-850	0.09-0.64	[40]

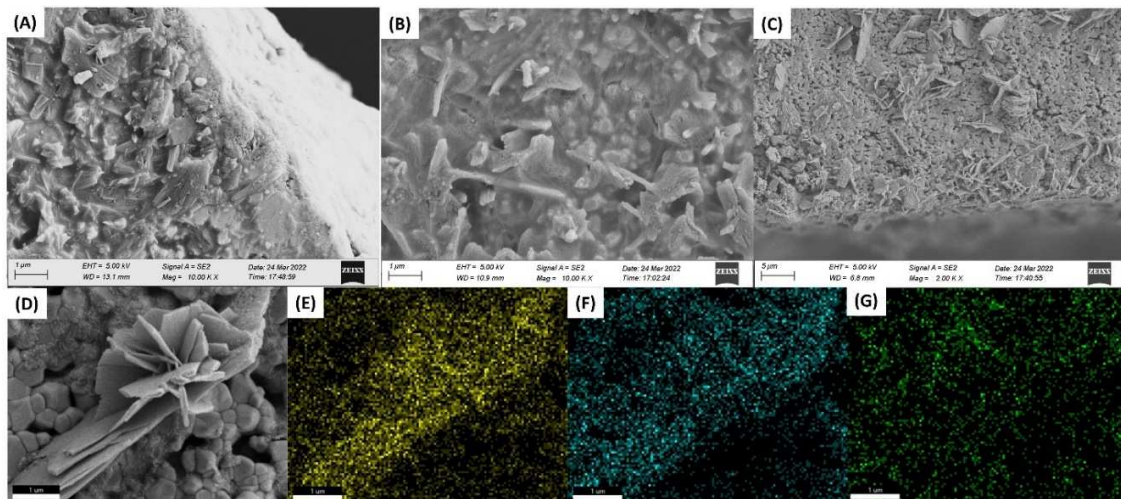
Ce <sub>0.8</sub> Sm <sub>0.2</sub> O <sub>2-δ</sub> (SDC)	0.1–0.15	0.75	0.2	500-700	0.09-1.79	[41]
SDC-SDC/La <sub>2</sub> NiO <sub>4</sub> (LNO)	~0.23	1.32	0.5	550-750	0.36-2.3	[30]
GDC	0.5	4.0	0.05	650	0.35-0.55	This work

1

2 *Post-test analysis of the membrane*

3 After the stability tests, the surface and internal structures of the membrane were further examined  
4 by SEM/EDS. Figure 9(A) and (B) shows that the interior of the membrane remained dense  
5 without significant loss of MC during the test, which supports the stable J<sub>CO<sub>2</sub></sub> observed. However,  
6 on the permeate side surface, some flake like materials are found; see Figure 9(C) and 9(D). The  
7 EDS analysis in Figure 9(E) and 9(F) indicates that the flakes are rich in C and O, implying a likely  
8 carbonate phase even though EDS cannot detect Li. The fact that the flakes lack Na, as shown in  
9 Figure 9(G), infers that it might be only Li-rich carbonate such as Li<sub>2</sub>CO<sub>3</sub> and LiHCO<sub>3</sub>. We have  
10 previously observed the same phenomenon.[35] We then conclude that the flake like materials  
11 might be the product of hydrated carbonate recrystallized during cooling.

12



1 Figure 9. Cross-sectional views of (A) feed, (B) middle, and (C) permeate side of GDC-MC tubular  
2 membrane and (D) close look at flakes by SEM and elemental mapping by EDS: (E) O, (F) C and  
3 (G) Na.

4

5

#### 4. Conclusions

6 In this study, a tubular GDC-MC membrane with an active surface area of 4 cm<sup>2</sup> has been  
7 successfully fabricated via a CIP method. With 5%CO<sub>2</sub>-N<sub>2</sub> as the retentate gas and dry Ar as the  
8 permeate gas, the membrane exhibits J<sub>CO<sub>2</sub></sub>= 0.35 mL/min·cm<sup>2</sup> and CCR=28% at 650 °C. The J<sub>CO<sub>2</sub></sub>  
9 and CCR are further enhanced by moistening the permeate Ar gas, reaching 0.45-0.55 mL/min·cm<sup>2</sup>  
10 and 37-42%, respectively, at 3-15% H<sub>2</sub>O. The measured H<sub>2</sub>O flux at the retentate side matches, in  
11 general, with the measured CO<sub>2</sub> flux at the permeate side, supporting the co-transport mechanism  
12 of CO<sub>2</sub> and H<sub>2</sub>O in the MC phase. As CO<sub>2</sub> concentration in the retentate gas increases, CO<sub>2</sub> flux  
13 increases correspondingly, but CCR decreases, implying the limited capability of the membrane  
14 of the current geometry (small surface area) to capture high concentration of CO<sub>2</sub>. With increasing  
15 the length and diameter of the membrane, the CO<sub>2</sub> capturing ability (or CCR) is expected to  
16 improve. The post-test analysis indicates that the membrane remains dense without sign of MC  
17 loss after testing. The flake-like substance on the surface of the permeate side surface are observed,  
18 likely an indicator of hydrated products.

#### 19 Acknowledgement

20 We would like to thank US Department of Energy, Office of Fossil Energy, National Energy  
21 Technology Laboratory (Award # DE-FE-0031634), and National Science Foundation (Award #  
22 CBET-1924095) for supporting this work.

## 1 **References**

- 2 [1] <https://www.eia.gov/todayinenergy/detail.php?id=34172#>, Natural gas generators make up  
3 the largest share of overall U.S. generation capacity, in, 2020.
- 4 [2] o.C.e.p.  
5 <https://www.eia.gov/tools/faqs/faq.php?id=74&t=11#:~:text=In%202019%2C%20total%20U.S.%20electricity,How%20much%20carbon%20dioxide%20is%20produced%20per%20kilowatt%20hour%20of%20U.S.%20electricity>, How much carbon dioxide is produced per kilowatthour of U.S. electricity  
6 generation?, in, 2020.
- 7 [3] Y.G. Zhang, J.Y.G. Chan, Sustainable chemistry: imidazolium salts in biomass conversion  
8 and CO<sub>2</sub> fixation, *Energy & Environmental Science*, 3 (2010) 408-417.
- 9 [4] S. Smart, C.X.C. Lin, L. Ding, K. Thambimuthu, J.C.D. da Costa, Ceramic membranes for  
10 gas processing in coal gasification, *Energy & Environmental Science*, 3 (2010) 268-278.
- 11 [5] Q.A. Wang, J.Z. Luo, Z.Y. Zhong, A. Borgna, CO<sub>2</sub> capture by solid adsorbents and their  
12 applications: current status and new trends, *Energy & Environmental Science*, 4 (2011) 42-55.
- 13 [6] A.Z. Robert James, Dale Keairns, Marc Turner, Mark Woods, Norma Kuehn, COST AND  
14 PERFORMANCE BASELINE FOR FOSSIL ENERGY PLANTS VOLUME 1: BITUMINOUS  
15 COAL AND NATURAL GAS TO ELECTRICITY, in: NETL-PUB-22638, 2019.
- 16 [7] D.R.L.a.H.W.P. D. Shekhawal, A review of carbon dioxide selective membranes, in: NETL  
17 (Ed.), 2003.
- 18 [8] T.Y. H. Kawamura, N. N. Balagopal, K. Nakagawa and S. Nakao, Dual-Ion Conducting  
19 Lithium Zirconate-Based Membranes for High Temperature CO<sub>2</sub> Separation, *J. Chem. Eng.*  
20 *Jpn.*, 38 ( 2005) 322-328.
- 21 [9] E.J.G.a.T. O'Brien, Review of novel methods for carbon dioxide separation from flue and  
22 fuel gases, *Fuel Proc. Tech.*, 86 (2005) 1423-1434.
- 23 [10] N.Y. Du, H.B. Park, M.M. Dal-Cin, M.D. Guiver, Advances in high permeability polymeric  
24 membrane materials for CO<sub>2</sub> separations, *Energy & Environmental Science*, 5 (2012) 7306-  
25 7322.
- 26 [11] T.F. J. D. Figueroa, S. Plasynski, H. McIlvried and R.D. Srivastava, Advances in CO<sub>2</sub>  
27 capture technology--The US Department of Energy's carbon sequestration program, *Int. J. Green.*  
28 *Gas Cntrl.*, 2 (2008) 9-20.
- 29 [12] R. Quinn, J.B. Appleby, G.P. Pez, New Facilitated Transport Membranes for the Separation  
30 of Carbon-Dioxide from Hydrogen and Methane, *Journal of Membrane Science*, 104 (1995) 139-  
31 146.
- 32 [13] M.R. Cerón, L.S. Lai, A. Amiri, M. Monte, S. Katta, J.C. Kelly, M.A. Worsley, M.D.  
33 Merrill, S. Kim, P.G. Campbell, Surpassing the conventional limitations of CO<sub>2</sub> separation  
34 membranes with hydroxide/ceramic dual-phase membranes, *Journal of Membrane Science*, 567  
35 (2018) 191-198.
- 36 [14] W. Xing, A. Støre, Contact angle screening and asymmetric dual-phase CO<sub>2</sub> separation  
37 membranes, *Journal of Membrane Science*, 652 (2022) 120447.
- 38 [15] J. Fabian-Anguiano, M. Ramírez-Moreno, H. Balmori-Ramírez, J. Romero-Serrano, I.  
39 Romero-Ibarra, X. Ma, J. Ortiz-Landeros, Syngas production with CO<sub>2</sub> utilization through the  
40 oxidative reforming of methane in a new cermet-carbonate packed-bed membrane reactor,  
41 *Journal of Membrane Science*, 637 (2021) 119607.
- 42 [16] L. Grima, G.A. Mutch, P.B. Oliete, W. Bucheli, R. Merino, E.I. Papaioannou, J. Bailey, M.  
43 Kok, D. Brett, P. Shearing, High CO<sub>2</sub> permeability in supported molten-salt membranes with  
44

1 highly dense and aligned pores produced by directional solidification, *Journal of Membrane*  
2 *Science*, 630 (2021) 119057.

3 [17] M. Starykevich, A. Jamale, K. Yasakau, F. Marques, Novel molten phase route for  
4 composite CO<sub>2</sub> separation membranes, *Journal of Membrane Science*, (2022) 120806.

5 [18] P. Zhang, J. Tong, K. Huang, X. Zhu, W. Yang, The current status of high temperature  
6 electrochemistry-based CO<sub>2</sub> transport membranes and reactors for direct CO<sub>2</sub> capture and  
7 conversion, *Progress in Energy and Combustion Science*, 82 (2021).

8 [19] J.H.P. S. J. Chung, D. Li, J.-I. Ida, I. Kumakiri, and Jerry Y. S. Lin, Dual-Phase Metal-  
9 Carbonate Membrane for High-Temperature Carbon Dioxide Separation, *Ind. Eng. Chem. Res.*,  
10 44 (2005) 7999.

11 [20] L. Zhang, N. Xu, X. Li, S. Wang, K. Huang, W.H. Harris, W.K.S. Chiu, High CO<sub>2</sub>  
12 permeation flux enabled by highly interconnected three-dimensional ionic channels in selective  
13 CO<sub>2</sub> separation membranes, *Energy & Environmental Science*, 5 (2012) 8310.

14 [21] N. Xu, X. Li, M.A. Franks, H. Zhao, K. Huang, Silver-molten carbonate composite as a new  
15 high-flux membrane for electrochemical separation of CO<sub>2</sub> from flue gas, *Journal of Membrane*  
16 *Science*, 401-402 (2012) 190-194.

17 [22] S. Wang, J. Tong, L. Cui, P. Zhang, F. Zhou, A layered perovskite La<sub>1-5</sub>Sr<sub>0.5</sub>NiO<sub>4±δ</sub>-  
18 molten carbonate dual-phase membrane for CO<sub>2</sub> capture from simulated flue gas, *Journal of*  
19 *Membrane Science*, 647 (2022) 120278.

20 [23] O. Ovalle-Encinia, H.-C. Wu, T. Chen, J.Y. Lin, CO<sub>2</sub>-permselective membrane reactor for  
21 steam reforming of methane, *Journal of Membrane Science*, 641 (2022) 119914.

22 [24] S.G. Carvalho, E.N. Muccillo, F.C. Fonseca, M. Müller, F. Schulze-Küppers, S. Baumann,  
23 W.A. Meulenbergh, O. Guillon, R. Muccillo, Tape-casting and freeze-drying gadolinia-doped  
24 ceria composite membranes for carbon dioxide permeation, *Journal of Membrane Science*, 648  
25 (2022) 120355.

26 [25] L.M. Robeson, The upper bound revisited, *Journal of Membrane Science*, 320 (2008) 390-  
27 400.

28 [26] M.M. Dal-Cin, A. Kumar, L. Layton, Revisiting the experimental and theoretical upper  
29 bounds of light pure gas selectivity-permeability for polymeric membranes, *Journal of*  
30 *Membrane Science*, 323 (2008) 299-308.

31 [27] P. Zhang, J. Tong, K. Huang, A self-forming dual-phase membrane for high-temperature  
32 electrochemical CO<sub>2</sub> capture, *Journal of Materials Chemistry A*, 5 (2017) 12769-12773.

33 [28] P. Zhang, J. Tong, K. Huang, Self-Formed, Mixed-Conducting, Triple-Phase Membrane for  
34 Efficient CO<sub>2</sub>/O<sub>2</sub> Capture from Flue Gas and in Situ Dry-Oxy Methane Reforming, *ACS*  
35 *Sustainable Chemistry & Engineering*, 6 (2018) 14162-14169.

36 [29] Z. Xu, Q. Zheng, S. Wang, Z. Zhang, Z. Liu, G. Zhang, W. Jin, Fabrication of molten  
37 nitrate/nitrite dual-phase four-channel hollow fiber membranes for nitrogen oxides separation,  
38 *Journal of Membrane Science*, 635 (2021) 119506.

39 [30] T. Chen, Y. Xu, Y. Zhang, Y. Gong, Y. Zhang, J.Y. Lin, Double-layer ceramic-carbonate  
40 hollow fiber membrane with superior mechanical strength for CO<sub>2</sub> separation, *Journal of*  
41 *Membrane Science*, (2022) 120701.

42 [31] H.-C. Wu, Z. Rui, J.Y. Lin, Hydrogen production with carbon dioxide capture by dual-phase  
43 ceramic-carbonate membrane reactor via steam reforming of methane, *Journal of Membrane*  
44 *Science*, 598 (2020) 117780.

- 1 [32] X. Dong, Y. Lin, Catalyst-free ceramic-carbonate dual phase membrane reactor for  
2 hydrogen production from gasifier syngas, *Journal of Membrane Science*, 520 (2016) 907-913.
- 3 [33] O. Ovalle-Encinia, J.Y. Lin, High-pressure CO<sub>2</sub> permeation properties and stability of  
4 ceramic-carbonate dual-phase membranes, *Journal of Membrane Science*, 646 (2022) 120249.
- 5 [34] Y. Lin, A. Burggraaf, Experimental studies on pore size change of porous ceramic  
6 membranes after modification, *Journal of membrane science*, 79 (1993) 65-82.
- 7 [35] K. Zhang, S. Sun, N. Xu, K. Huang, H<sub>2</sub>O-enhanced CO<sub>2</sub> transport through a proton  
8 conducting ceramic-molten carbonate dual-phase membrane, *Journal of Membrane Science*, 650  
9 (2022) 120421.
- 10 [36] L. Zhang, N. Xu, X. Li, S. Wang, K. Huang, W.H. Harris, W.K. Chiu, High CO<sub>2</sub>  
11 permeation flux enabled by highly interconnected three-dimensional ionic channels in selective  
12 CO<sub>2</sub> separation membranes, *Energy & Environmental Science*, 5 (2012) 8310-8317.
- 13 [37] S. Sun, Y. Wen, K.J.A.S.C. Huang, *Engineering*, A New Ceramic–Carbonate Dual-Phase  
14 Membrane for High-Flux CO<sub>2</sub> Capture, 9 (2021) 5454-5460.
- 15 [38] M. Zuo, S. Zhuang, X. Tan, B. Meng, N. Yang, S. Liu, Ionic conducting ceramic–carbonate  
16 dual phase hollow fibre membranes for high temperature carbon dioxide separation, *Journal of*  
17 *Membrane Science*, 458 (2014) 58-65.
- 18 [39] S. Zhuang, Y. Li, M. Zuo, X. Tan, B. Meng, N. Yang, S. Liu, Dense composite electrolyte  
19 hollow fibre membranes for high temperature CO<sub>2</sub> separation, *Separation and Purification*  
20 *Technology*, 132 (2014) 712-718.
- 21 [40] X. Jiang, J. Zhu, Z. Liu, S. Guo, W. Jin, CO<sub>2</sub>-tolerant SrFe<sub>0.8</sub>Nb<sub>0.2</sub>O<sub>3-δ</sub>-carbonate dual-  
22 phase multichannel hollow fiber membrane for CO<sub>2</sub> capture, *Industrial & Engineering*  
23 *Chemistry Research*, 55 (2016) 3300-3307.
- 24 [41] T. Chen, Z. Wang, J. Hu, M.H. Wai, S. Kawi, Y. Lin, High CO<sub>2</sub> permeability of ceramic-  
25 carbonate dual-phase hollow fiber membrane at medium-high temperature, *Journal of Membrane*  
26 *Science*, 597 (2020) 117770.

27

